Journal of Materials Chemistry B

ROYAL SOCIETY OF CHEMISTRY

PAPER

View Article Online
View Journal | View Issue

Cite this: J. Mater. Chem. B, 2023, 11, 8788

Bioinspired mechanically stable all-polysaccharide based scaffold for photosynthetic production†

Tuuli Virkkala,[a] Sergey Kosourov,[b] Ville Rissanen,[a] Vilja Siitonen,[b] Suvi Arola,[a] Yagut Allahverdiyeva *[b] and Tekla Tammelin *[a]

Received 24th April 2023,
Accepted 19th August 2023

DOI: 10.1039/d3tb00919j

rsc.li/materials-b

We demonstrate the construction of water-stable, biocompatible and self-standing hydrogels as scaffolds for the photosynthetic production of ethylene using a bioinspired all-polysaccharidic design combining TEMPO-oxidised cellulose nanofibers (TCNF) and a cereal plant hemicellulose called mixed-linkage glucan (MLG). We compared three different molecular weight MLGs from barley to increase the wet strength of TCNF hydrogels, and to reveal the mechanisms defining the favourable interactions between the scaffold components. The interactions between MLGs and TCNF were revealed *via* adsorption studies and interfacial rheology investigations using quartz crystal microbalance with dissipation monitoring (QCM-D). Our results show that both the MLG solution stability and adsorption behaviour did not exactly follow the well-known polymer adsorption and solubility theories especially in the presence of co-solute ions, in this case nitrates. We prepared hydrogel scaffolds for microalgal immobilisation, and high wet strength hydrogels were achieved with very low dosages of MLG (0.05 wt%) to the TCNF matrix. The all-polysaccharic biocatalytic architectures remained stable and produced ethylene for 120 h with yields comparable to the state-of-the-art scaffolds. Due to its natural origin and biodegradability, MLG offers a clear advantage in comparison to synthetic scaffold components, allowing the mechanical properties and water interactions to be tailored.

1. Introduction

Plant cell walls are strong natural composites formed by a fibrous backbone and an amorphous matrix.[1,2] The backbone consists of cellulose fibrils that interact with diverse and structurally complex matrix polysaccharides, such as hemicelluloses, to form highly durable and load-bearing networks with efficient water and nutrient transport properties.[3,4] In addition to the interactions with cellulose, hemicelluloses interact strongly with water, which is a crucial constituent of the plant cell wall influencing its structural and mechanical properties.[5,6] Inspired by the cell wall architecture, hemicelluloses have been studied for their interactions with cellulosic materials in the development of polysaccharide-based structures for various applications.[7–9] Recently, mixed-linkage glucans (MLGs) *i.e.*, hemicelluloses found in cell walls of grassy plants such as cereals,[10] have gained attention due to their intrinsic interactions with cellulose,[11] unique ability to efficiently gel nanocellulosic materials even at ultra-low solids contents,[12] and hydrate cellulosic networks due to their strong water interactions.[13]

Cell factories from photosynthetic microorganisms, *i.e.* eukaryotic microalgae and procaryotic cyanobacteria, have been widely researched as an alternative to petroleum-based fossil resources in the production of sustainable chemicals and fuels.[14,15] Despite the promise of photosynthetic microbial cell factories, technical hurdles associated with suspension cultures, such as the self-shading effect leading to low light utilisation efficiency as well as high water and energy consumption, have limited harnessing their theoretical potential in chemicals and fuels production.[16–18] Thin-layer immobilisation, *i.e.* binding the cells within a gel-like matrix, has been suggested to help address these difficulties.[17,19–21] Previously, nanocellulose-based materials have been demonstrated as a viable alternative to conventionally used alginate-based matrices,[16,22,23] since alginate-based matrices have their shortcomings in terms of mechanical stability especially in media with high content of chelating agents.

In addition to unique mechanical and colloidal properties[24,25] and beyond their biocompatibility, nanocelluloses are interesting for biological and biomimicking applications due to their life-sustaining property.[26] Fundamentally, cellulose has a hierarchical structure with individual molecules packed into microfibrils, further into microfibril bundles, and ultimately cellulose fibers.[27]

Due to the mechanical properties, optical transparency, and highly hygroscopic nature, TEMPO-oxidised cellulose nanofibers

[a] VTT Technical Research Centre of Finland Ltd, VTT, PO Box 1000, FI-02044 Espoo, Finland. E-mail: tekla.tammelin@vtt.fi
[b] Molecular Plant Biology, Department of Life Technologies, University of Turku, FI-20014 Turku, Finland. E-mail: allahve@utu.fi

† Electronic supplementary information (ESI) available. See DOI: https://doi.org/10.1039/d3tb00919j

(TCNFs)[28] are an attractive choice for immobilisation of photosynthetic microorganisms that require both an aqueous environment and sufficient light for growth.[16,22] The challenge with TCNF gels is in their poor aqueous stability, which can be increased by various cross-linking strategies.[29] Di- or multivalent metal cations, for example Ca^{2+}, have been shown to efficiently improve the wet strength of TCNF-based structures,[30] but the ionic cross-linking is reversible by nature, limiting the feasibility of this strategy when submerged in nutrient-rich growth medium containing chelating agents.[22] Addition of synthetic polyvinyl alcohol (PVA) has also been suggested to improve the wet strength of TCNF.[31] However, this strategy has significance mainly in dry films since formation of the cross-linked covalent ester bond requires efficient drying.[32] Furthermore, PVA constitutes a possible source of microplastics in the environment due to its limited biodegradability[33] and finding bio-based alternatives is favourable. Therefore, mixed-linkage glucans are interesting as an alternative bioinspired approach, mimicking the natural architecture and function of the grass cell wall.

The linear MLG homopolysaccharides consist of consecutive glucose units connected by two types of linkages: β-(1,4)-linked glucoses form cellotriosyl and cellotetraosyl units that are joined together by single interspersed β-(1,3)-linkages.[34] The cellotriosyl and cellotetraosyl units constitute approximately 58–72% and 21–34% of the polymer, respectively.[35] Additionally, MLGs also contain larger segments (5–11 glucose units), comprising around 10–20% of the polymer.[36] This type of linking results in an irregular shape that renders the polymer flexible and soluble in water and prevents intermolecular alignment of MLGs into structured microfibrils.[37,38] Together with a high degree of polymerisation, however, the asymmetric conformation allows MLGs to form a gel-like matrix between cellulose fibrils in the cell wall.[39] Besides providing additional strength coupled with a certain extent of flexibility and elasticity, the gel-like matrix is thought to provide the cell wall with porosity, which is essential for water and nutrient exchange.[40] These features make MLGs an interesting component for leaf-inspired nanocellulose-based scaffolds for biocatalytic solid-state photosynthetic cell factories (SSPCFs).

This paper demonstrates a bioinspired, all-polysaccharidic scaffold for SSPCFs obtained from bio-based components, cellulose nanofibers (TCNF) and hemicellulose from barley (MLG), in a design that mimics the composition and architecture of the plant cell wall (Fig. 1). The aim is to reveal the mechanism of how MLGs contribute to TCNF gel wet strength and stability. For this, we conduct a rigorous interfacial and bulk investigation to clarify MLG binding and stability of interactions as well as gel strength in physiological conditions. Quartz crystal microbalance with dissipation monitoring (QCM-D) is applied to study adsorption of three commercially available MLGs with different molecular weights on TCNF surfaces. We model the viscoelastic properties of the MLG adlayers by fitting the Voigt model[41] to the adsorption and energy dissipation data. The swelling and water binding of the adsorbed TCNF–MLG layers are considered due to the key role of water interactions at the hemicellulose–cellulose interface.[5,6] Furthermore, we attempt to relate the interfacial rheology results to bulk rheological properties to gain in-depth understanding of the materials' macroscale properties. Finally, we highlight the performance of TCNF–MLG scaffolds with embedded ethylene-producing cyanobacteria in challenging submerged production conditions for a prolonged time span

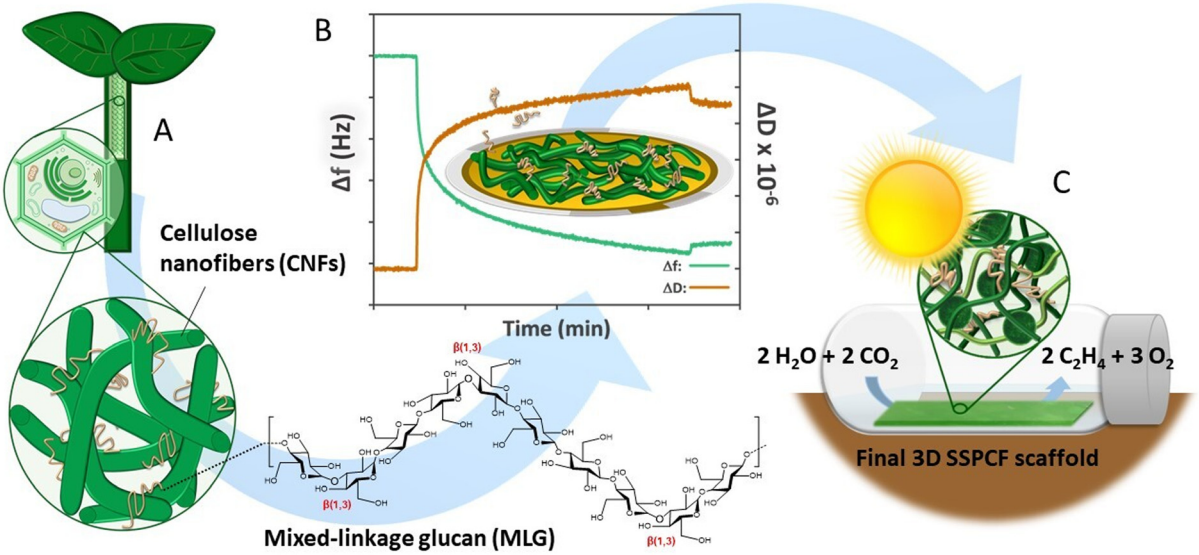

Fig. 1 Conceptual view of the design steps of a bioinspired scaffold for photosynthetic production from mixed-linkage glucan (MLG) and nanocellulose: (A) The native cell wall structure of cereal plants with MLGs interlaced in the cellulose network was used as inspiration. (B) An interfacial study using quartz crystal microbalance with dissipation monitoring (QCM-D) and nanocellulose ultra-thin films was conducted to understand the component interactions in an aqueous environment. (C) Nanocellulose and MLGs were combined to fabricate the final 3D scaffold architecture and its performance was demonstrated with an ethylene bioproduction assay.

of 120 h. The research paves the way towards a bioinspired, fully polysaccharide-based, and tailored scaffold for entrapment of engineered cyanobacteria as biocatalytic architectures for photosynthetic chemicals production.

2. Experimental

2.1. Materials

2.1.1. TEMPO-oxidised cellulose nanofibers. Never-dried bleached softwood pulp (spruce/pine mixture) sourced from a Finnish pulp mill was TEMPO-oxidised as described by Saito *et al.*[28] in alkaline conditions with hypochlorite and TEMPO as catalysts. The anionic charge of the oxidised pulp was determined with standard conductometric titration (SCAN 65:02)[42] as 1.45–1.52 mmol g^{-1}. The oxidised pulp was washed and fibrillated into CNF (hereby called TCNF) with a microfluidizer (Microfluidics Int., USA) with two Z-type chambers with 400 and 100 μm diameters, respectively. The fluidization was done in two passes at 1850 bar operating pressure yielding TCNF with a viscous and transparent appearance and a final consistency of approximately 1 wt%. The TCNF was stored refrigerated.

2.1.2. MLG solutions. Low viscosity (LV), medium viscosity (MV) and high viscosity (HV) barley mixed-linkage glucans with weight average molecular weights (M_w) of 179 kg mol^{-1}, 238 kg mol^{-1}, and 495 kg mol^{-1} (hereby called LVMLG, MVMLG, and HVMLG) were purchased from Megazyme (catalog numbers P-BGBL, P-BGBM, and P-BGBH). 0.01 wt% and 1 wt% solutions for surface sensitive measurements and hydrogel films, respectively, were prepared according to manufacturer's instructions: the powders were wetted with ethanol (Etax A, Altia Industrial) before addition of Milli-Q water. The solutions were heated to boiling and stirred until fully transparent indicating that MLGs were completely dissolved. The solutions were allowed to cool to room temperature and their volumes were adjusted to obtain the desired final concentrations. The 1 wt% stock solutions were stored at room temperature and resolubilised by heating and stirring prior to use in the hydrogel matrices as the MLGs tend to self-associate and precipitate over time.[43]

2.1.3. Cyanobacterial strains and growth conditions. Wild-type cyanobacterial *Synechocystis* sp. PCC 6803 cells (hereby Synechocystis) were used for the rheological measurements and photosynthetic activity monitoring. The cell cultures were maintained at 23 °C in BG-11 medium prepared according to Rippka *et al.*[44] and buffered with 5 mM HEPES-NaOH (pH 7.5). The cultures were agitated with a rotary shaker (110 rpm) and illuminated with fluorescent lamps (Philips Master TL5 HO 39W/865) providing approximately 50 μmol photons m^{-2} s^{-1} photosynthetic active radiation (PAR) to the cells. The illumination was set to operate in a cycle of 16 h light followed by 8 h of darkness. The cultures were cultivated under normal air atmosphere. For the experiments, the cells were harvested by centrifugation at 10 000*g* for 15 min. The cell pellets were resuspended in fresh BG-11 medium to obtain culture with an optical density (OD_{720}) of approximately 1.0 as measured with AquaPen-C AP-C 100 handheld fluorometer (Photon Systems Instruments, Czech Republic).

For ethylene production experiments, an ethylene-producing cyanobacterium clone (S5) by heterologous expression of ethylene forming enzyme (Efe) from *Pseudomonas syringae* in *Synechocystis* sp. PCC 6803 (shortly, Synechocystis *efe*)[45,46] was applied. The cells were maintained in BG-11 medium containing 20 mM HEPES-NaOH (pH 7.5) at 30 °C supplemented with 25 μg mL^{-1} spectinomycin and 10 μg mL^{-1} chloramphenicol. The cultures were agitated on a rotary shaker (120 rpm) in a growth chamber (MLR-351, versatile environmental test chamber Sanyo, Japan) with 1% CO_2 in the atmosphere. The cells were illuminated continuously with fluorescent light of about 35 μmol photons m^{-2} s^{-1} (Philips Master TL-D 36W/865). Experimental cultures were grown without antibiotics and without agitation in 1 L flat round neck Roux type flask (DURAN®, Schott, DWK Life Sciences GmbH) in BG-11 medium. These cultures were continuously bubbled using sterile filtered air supplemented with 1% CO_2 (0.2 μm, Acro 37 TF, Gelman Sciences, USA). The cells were collected at OD_{750} 1.4–1.9 by centrifugation at 5000 g for 10 min (Avanti JXN-26, JA10, Beckman Coulter). The cells were resuspended in fresh BG-11 and the OD_{750} was adjusted to 1.0 prior to immobilisation using the UV-1800 spectrophotometer (Shimadzu, Japan).

2.1.4. Other materials. All used chemicals were of analytic grade and used as received. TEMPO, solid NaBr, aqueous 10% NaClO, and $CaCl_2$ (99%, #C7902) were purchased from Sigma-Aldrich. 0.1 M NaOH solution was obtained from Fluka Analytical. Ultrapure water (18.2 MΩ cm) was prepared with a Milli-Q purification unit (QPAK® 1, Millipore). Conductivities were measured with Jenway 4510 conductivity meter (Cole-Parmer, Vernon-Hills, IL, USA). A commercial Teflon (PTFE) film (Etra, Finland) was used as support for the hydrogel films, and the PTFE film was surface treated prior to use with LabTec Corona Lab System (Tantec, Lunderskov, Denmark) using 28.0 kV voltage, 200 W power, and 100% electrode matching. Poly(ethylene imine) (PEI) solution in water (polyethylenimine, branched, 33 wt%, M_w = 50 000–100 000, 06090-100) was purchased from Polysciences Inc. (Warrington, PA, USA). AT-cut gold-coated quartz crystal sensors (QSX 301) with a fundamental resonance frequency f_0 = 5 MHz and a sensitivity constant C = 0.177 mg m^{-2} Hz^{-1} were obtained from Biolin Scientific AB, Sweden.

2.2. Methods

2.2.1. Dynamic light scattering (DLS) and ζ-potential. DLS and ζ-potential were measured to assess the size and charge of MLG polymers. For the measurements, three solutions of each MLG were prepared. The MLGs were dissolved in water in 0.01 wt% concentration and the pH of the solutions was adjusted to approximately 7.5 and 8.5. Each MLG was also dissolved in BG-11 buffer (pH ~ 7.5) in the same concentration. Freshly prepared solutions were filtered through a 0.45 μm filter membrane prior to measurements to remove large particles. For DLS, disposable polystyrene cuvettes (#67.754, Sarstedt AG & Co. KG, Germany) were used, and the samples were analysed with a Zetasizer NanoZS apparatus (Malvern Panalytical, Malvern, UK) with a 633 nm laser using backscatter angle detection

of 173°. DLS was performed at 23 °C, and a refractive index increment of 0.146 mL g^{-1} was used for the MLGs. ζ-Potential measurements were carried out by electrophoretic light scattering in the same equipment using disposable folded capillary cells (DTS1070, Malvern Panalytical, Malvern, UK), and a -42 ± 4 mV standard was used as a control for the device. At least five repetitions of each sample were measured both for particle size and ζ-potential determination.

2.2.2. Preparation of TCNF ultrathin films for QCM-D investigations. TCNF thin films were prepared according to Hakalahti *et al.*[47] with slight modifications to the original procedure.[48] Briefly, gold-coated sensor crystals were rinsed with Milli-Q water, dried with nitrogen gas, and cleaned with UV/ozone ProCleaner™ (BioForce Nanosciences Inc., Ames, IA, USA) for 15 min. 0.1 wt% PEI, acting as an anchoring polymer, was drop casted on the cleaned sensor surfaces for 30 min. The sensors were rinsed and dried afterwards. 0.15 wt% suspension of TCNF was prepared by diluting 1 wt% TCNF with Milli-Q water and ultrasonicated with Branson 450 Digital Sonifier at 25% amplitude for 2 min. 200 μL of TCNF suspension was spin-coated onto the PEI-coated sensors with WS-400BZ-6NPP/Lite spin-coater (Laurell Technologies Corporation, North Wales, PA, USA) at 3000 rpm for 1.5 min followed by drying the sensors in 80 °C for 7 min to ensure fibril attachment.

2.2.3. Interfacial interactions – Adsorption of MLGs on TCNF *via* quartz crystal microbalance with dissipation monitoring (QCM-D). Quartz crystal microbalance with dissipation monitoring (QCM-D E4, Q-Sense AB) was used to study the adsorption of MLGs on TCNF surfaces at the solid–liquid interface. In QCM-D, a pulsating electric field is applied on a piezoelectric quartz crystal sensor that oscillates at a specific fundamental resonance frequency f_0 and its overtones. As the total mass of a layer covering the sensor surface increases during adsorption, the resonance frequency changes to f. If the adsorbed layer can be considered even in distribution, rigidly adhered, fully elastic, and small in mass compared to the sensor crystal, the change in frequency, Δf, is directly proportional to a change in areal mass according to the Sauerbrey equation (eqn (1)):

$$\Delta m = -C\frac{\Delta f}{n} \quad (1)$$

where Δm, Δf, C, and n stand for the mass change per unit area, change in resonance frequency ($f - f_0$), sensitivity constant of the sensor, and overtone number (n = 1, 3, 5, 7, 9, 11, 13), respectively. Whether an adsorbed layer is rigid or soft (water-rich) can be determined by measuring several frequencies and dissipation, which is not possible if only the frequency response is observed. By periodically cutting off the voltage at the same time, frictional losses occur in the covering layer that causes the oscillation to decrease gradually and the oscillation amplitude to dampen if the material is not fully elastic. This energy dissipation factor, D, is defined as (eqn (2)):

$$D = \frac{E_{\text{dissipation}}}{2\pi E_{\text{storage}}} \quad (2)$$

where $E_{\text{dissipation}}$ represents the dissipated energy and E_{storage} the total energy stored during a single cycle of oscillation. The change in dissipation factor, $\Delta D = D - D_0$, measured by the QCM-D device can be used as a qualitative measure of layer rigidity and softness. D_0 is the dissipation factor of the pure crystal immersed in solvent. For a fully elastic layer, $\Delta D \leq 1 \times 10^{-6}$ and the overtones of Δf and ΔD do not significantly diverge.

The spincoated TCNF thin films were allowed to stabilise in Milli-Q water overnight prior to the measurement to allow only the effect of MLG adsorption on frequency and dissipation to be investigated. During the experiment, water was first introduced to the flow cells at a rate of 0.1 mL min^{-1} at 23 °C for ≥30 min to obtain a steady baseline. Then, water was replaced with 0.01 wt% MLG solutions. The change in frequency (Δf) and change in dissipation (ΔD) were followed for approximately 5 h (300 min) until the equilibrium was reached. Finally, the flow cells were rinsed with water for ≥30 min. For LVMLG, which possessed the most promising mechanical properties based on the preliminary studies, the same experiment was repeated by using BG-11 as a buffer to investigate adsorption behaviour also in nutrient-rich growth medium. Similarly, the TCNF model films were first allowed to stabilize in BG-11 overnight, followed by the adsorption of LVMLG solution prepared in BG-11. The data represented was acquired with the third overtone (15 MHz, f_0 = 5 MHz, n = 3).

2.2.4. Interfacial rheology – Viscoelastic modelling of adsorption data. Different models can be used to interpret QCM-D data with respect to adsorbed mass and structural changes of the adsorbed layer. The Voigt model described by Voinova *et al.*[41] is useful to describe the viscoelastic properties of adsorbed layers on rigid surfaces in purely viscous and Newtonian solvents, assuming that the layer density and thickness are uniform, the viscoelastic properties are frequency independent, and that there is no slip between adsorbed layer and crystal during shearing. The model describes the adsorbed layer as a Voigt element by a frequency dependent complex equation when the layer is subjected to oscillating stress, and it can be used to estimate the shear viscosity, shear elastic modulus, and hydrodynamic thickness of the MLG layers as adsorption proceeds. The complex shear modulus of the formed layer is defined as (eqn (3)):

$$G = G' + iG'' = \mu_f + 2\pi i f \eta_f = \mu_f(1 + 2\pi i f \tau_f) \quad (3)$$

where η_f represents the shear viscosity, μ_f the shear elastic modulus, f the oscillation frequency, and τ_f the characteristic relaxation time of the film. The changes in frequency and dissipation factor were fitted to the model at 15, 25, and 35 MHz *i.e.*, at n = 3, 5, and 7 overtones, using the Dfind program provided by Biolin Scientific AB with the assumed layer density of 1.05 g cm^{-3}.

2.2.5. Determination of areal masses of dry TCNF–MLG thin films by QCM-D. The amount of adsorbed MLG at the solid–air interface was determined as described in Peresin *et al.*[49] with slight modifications. The spincoated TCNF thin films were used as the baseline. First, the frequency response of empty, clean sensor surfaces was measured in the QCM-D

device in air at 23 °C until Δf and ΔD reached stable levels. Then, the TCNF layers were spincoated on the sensor surfaces and the sensors were measured in air until stable values for Δf and ΔD were obtained. Following MLG adsorption on the same surfaces, the sensors were dried with nitrogen gas and placed back in the QCM-D measurement chamber to collect Δf and ΔD data. The measurement was continued until Δf and ΔD had stabilized. The data from each step was stitched together using QSoft software (Biolin Scientific), and the areal mass changes were calculated according to the Sauerbrey equation (eqn (1)). The third overtone (15 MHz, f_0 = 5 MHz, n = 3) was used for the calculations and all surfaces were assumed to have a constant layer density of 1.05 g cm^{-3}. The same procedure was repeated with three sensors for each MLG.

2.2.6. Atomic force microscopy (AFM). Atomic force microscopy (AFM) was used to study the topography of TCNF and TCNF–MLG thin films. The MultiMode 8 instrument (Bruker, Billerica, MA, USA) was operated in tapping mode using NCHV-A tapping mode silicon probes (Bruker), with a resonance frequency around 320 kHz, a spring constant k of 40 N m^{-1}, and tip radius of 8 nm. 1 × 1 μm height images were obtained and analysed with NanoScope Analysis v3.00 (Bruker) software. Other than flattening, no processing was made to the images. NanoScope Analysis was additionally used to obtain the root-mean-square roughness values (R_q) of the surfaces.

2.2.7. Preparation of thin self-standing TCNF hydrogel films and cell immobilisation procedure for rheological measurements, photosynthetic activity monitoring, and ethylene production assay. The methodology to prepare self-standing TCNF hydrogel films with MLG and Ca^{2+} (hereby MLG-Ca^{2+}-TCNF) was modified from Rissanen *et al.*[22] It should be noted that the utilised Ca^{2+} cross-linking procedure is a standard method to cross-link cell immobilisation matrices.[21,50] The $CaCl_2$ crosslinking is featured also in the TCNF-based immobilisation matrices where dual cross-linking based on polyvinyl alcohol and $CaCl_2$ has been investigated.[22,51] 1 wt% TCNF was mixed with either 0.01 wt%, 0.02 wt%, 0.05 wt%, 0.1 wt%, or 0.2 wt% LVMLG, MVMLG, or HVMLG. Then, Milli-Q water was added at 1 : 1 ratio with TCNF. The mixtures were homogenized with IKA T 18 digital Ultra-Turrax® at >10 000 rpm for at least 2 minutes until homogeneous. To get rid of air bubbles, the homogenized mixtures were centrifuged at 4500 G for 3 min. A handheld coating applicator with 2 mm gap was used to spread the gels into thin hydrogel films on coronated PTFE. An excess amount of 50 mM $CaCl_2$ was sprayed onto the gel films to further cross-link them.[16,22,30,51] To enhance cross-linking, the gel films were dried at +23 °C and 50% relative humidity (RH) until the original dry weight content of TCNF and MLG was reached, *i.e.*, until 50% of water from the diluted gels had evaporated. After the removal of the excess of water, the self-standing gel films were cut into circles with approximately 5 cm diameters and immersed in 50 mM $CaCl_2$ for 30 min. After this, $CaCl_2$ was removed, and the samples were submerged in Milli-Q water and left to swell overnight prior to the rheological measurements to obtain the aqueous conditions for wet strength characterisation.

Immobilisation of Synechocystis within MLG-Ca^{2+}-TCNF matrices for the rheology experiments and photosynthetic activity monitoring followed the same methodology as described above but using cell suspension instead of water. Cells were suspended in BG-11 growth medium with OD_{720} of 1.0 ± 0.1 (determined *via* AquaPen, Photon Systems Instruments, Czech Republic) and added to mixtures of 1 wt% TCNF and 0.01 wt% MV- and HVMLG or 0.05 wt% LVMLG in 1 : 1 ratio with TCNF. For rheology, control samples without the cells were prepared by replacing the cell suspension with BG-11 growth medium. The hydrogel films with the cells were then prepared like the MLG-Ca^{2+}-TCNF hydrogel films. The samples were cut as described above, immersed in $CaCl_2$ for 30 min, and left to swell in BG-11 overnight. For photosynthetic activity monitoring, the hydrogels were cut into 3 × 1 cm pieces, $CaCl_2$ treated, and stored on plates with BG-11.

For ethylene production studies, the MLG-Ca^{2+}-TCNF hydrogel films with Synechocystis *efe* were prepared as described above, except OD_{750} was adjusted to 1.0 using the UV-1800 spectrophotometer (Shimadzu, Japan). LVMLG in a concentration of 0.05 wt% was used in the final formulation. The hydrogel films were coated on the surface of a coronated PTFE support using the automatic film applicator (TQC Sheen) and 56 μm-, 100 μm- and 200 μm-graded Mayer rods to produce matrices with different thicknesses. 2 mm films were also prepared using the handheld applicator with 2 mm gap on the same support. Finally, the hydrogel matrices were stabilised by spraying 50 mM $CaCl_2$ over the surface of hydrogel layers, washed once in BG-11 medium, and the excess water was removed by evaporation yielding hydrogels with 50% water content. The films were placed in Petri dishes containing BG-11 and cultivated in the growth chamber at 30 °C under around 35 μmol photons m^{-2} s^{-1} fluorescent light and 1% CO_2 in air atmosphere. After 3 days of cultivation, the films were used for ethylene production experiments.

2.2.8. Characterisation of TCNF–MLG gel wet strength *via* rheological measurements. Wet mechanical properties of the MLG-Ca^{2+}-TCNF hydrogel films were investigated with small deformation oscillatory rheology. The oscillatory stress sweep measurements are described in detail in the ESI† (Experimental & Fig. S1). Shortly, the storage modulus (G', unit Pa) and loss modulus (G'', unit Pa) represent the capability of a material to store energy elastically and dissipate it as heat, respectively. The loss tangent or damping factor ($\tan\delta$) is given by the ratio of G'' to G' ($\tan\delta = G''/G'$). G', G'', and $\tan\delta$ denoted the rest behaviour of the materials in the linear viscoelastic (LVE) region. Critical stress denoting the onset of non-linear, irreversible deformation was determined from the stress/strain curve as the point in stress where a non-linear relationship between stress and strain was observed.

The rheological measurements were performed with an AR-G2 rheometer (TA Instruments, New Castle, DE, USA) at 22 °C. To avoid slip, a 40 mm cross-hatched plate-plate geometry was used. The measuring gap was adjusted to yield a normal force of 0.3–0.8 N between the sample and the rheometer, and the samples were let to relax under the measuring head for 2 min

prior to all measurements. Stress sweeps were conducted between 0.1–600 Pa oscillation range under a constant 0.1 Hz frequency, taking 10 points per measuring decade. At least five technical replicates with uniform thicknesses of 1000 ± 500 μm were measured for each sample and included in further analysis. TRIOS software (TA Instruments, New Castle, DE, USA) was used for operating the rheometer and data collection.

2.2.9. Assessing matrix biocompatibility *via* photosynthetic activity monitoring. The biocompatibility of MLG-Ca^{2+}-TCNF scaffolds was evaluated by immobilising the wild-type Synechocystis cells in the matrices and monitoring the cells' photosynthetic activity. The measurements were conducted with AquaPen (Photon Systems Instruments, Czech Republic) *via* quantum yield (QY) measurements. The device was set to use 620 nm red-orange excitation light with measuring and saturating light pulses of 0.009 μmol m^{-2} s^{-1} and 1500 μmol m^{-2} s^{-1}, respectively. In a light-adapted state, the QY given by $F_{v'}/F_{m'}$ is representative of the operating efficiency of photosystem II (PSII) photochemistry. $F_{m'}$ stands for the maximum fluorescence intensity and $F_{v'}$ for the variable fluorescence in the light-adapted state. $F_{v'}$ is obtained by subtracting $F_{t'}$, the steady-state chlorophyll fluorescence in the light, from $F_{m'}$. $F_{t'}$ and $F_{m'}$ are induced by the respective saturating and measuring light pulses of the device. The QY values were measured from three replicate 3 × 1 cm samples. The samples were stored on plates and supplemented with fresh BG-11 growth media every week during the monitoring period.

2.2.10. Ethylene production experiments. After 3 days of adaptation, MLG-Ca^{2+}-TCNF films with the embedded living Synechocystis *efe* cells were withdrawn from the growth chamber, washed once in fresh BG-11 medium, and cut into 3 × 1 cm strips. The strips were transferred in 23.5 mL gas-tight vials containing 3 mL of BG-11 supplemented with 200 mM $NaHCO_3$. The vials were sealed with Teflon-coated rubber stoppers and incubated in the growth chamber at 30 °C under 35 μmol photons m^{-2} s^{-1} continuous illumination provided by fluorescence lamps (Philips TL-D 36 W/865) from the top. The reaction of ethylene production was induced by introduction of 1 mM IPTG (isopropyl-β-D-thiogalactopyranoside) in vials.[45] The amount of ethylene was monitored every 24 h by using a gas chromatograph (GC, Clarus 580, PerkinElmer, Inc.) equipped with a capillary column (Carboxen 1010 PLOT 30 m × 0.53 mm) and a flame ionisation detector. The calibration was performed with the standard gas (1% v/v C_2H_4 in N_2, AGA, Finland). Calculations of ethylene content in vials considered the solubility of ethylene in water under the corresponding partial pressure of ethylene. The yield of ethylene was normalised to the film area and the chlorophyll *a* (Chl) content of films determined in the beginning of ethylene experiments.

2.2.11. Chl determination. Chl concentration was determined from three randomly selected 3 × 1 cm strips from the same MLG-Ca^{2+}-TCNF film preparation with embedded Synechocystis *efe* cells. The strips were incubated in 5 or 9 mL of 90–95% (v/v) methanol at +4 °C overnight in darkness. In some cases, the film strips were stored at −80 °C prior to addition of the solvent. Prior to measurements, 1 mL samples were moved to Eppendorf tubes and centrifuged using a tabletop centrifuge at full speed for 1 minute. Absorbance was measured at 665 and 730 nm using the UV-1800 spectrophotometer (Shimadzu, Japan). The 730 nm absorbance values were subtracted from the 665 readings and multiplied by 12.7 to get the Chl concentration.[52]

3. Results and discussion

3.1. Basic properties of MLGs – Polymers in aqueous solution

Table 1 lists the molecular weights of the three MLGs as given by the manufacturer, as well as ζ-potential values of 0.01 wt% MLG solutions in mV. To investigate the overall charge of MLGs under physiological conditions, the ζ-potentials were measured in water at pH ranges of 7.4–7.6 and 8.4–8.6, and in BG-11 growth medium with pH of 7.4–7.5. BG-11 medium contains a large number of dissolved salts used as a nutrient by photosynthetic cells.[44] Conductivities of ultrapure water and the growth medium are approximately 0.60 and 2400 μS cm^{-1}, respectively, indicating a high ionic strength of the nutrient rich medium. All aqueous solutions of MLGs displayed only very low negative ζ-potentials, and therefore MLG systems can be regarded as neutral polymers or at most weak anionic polyelectrolytes when dispersed in aqueous solution.

Fig. 2 represents size distributions of the MLGs as a function of light intensity percentage measured using DLS. The lower molecular weight LV- and MVMLG displayed a clear bimodal size distribution with two distinct peaks due to the strong tendency of the MLG polymers, and hemicelluloses more generally, to aggregate in solution.[53] The peaks around 35 and 43 nm for LV- and MVMLG, respectively, represent the individual polymer chains still present in the solution, whereas the peaks around 220 nm correspond to the formed polymer agglomerates. Aggregation seems to be reduced with increasing

Table 1 Basic properties of MLGs in aqueous solution. Standard deviations of ζ-potentials are based on at least five measurements

MLG type	M_w[a] (kg mol^{-1})	DP_w[b]	ζ-Potential[c] (mV)		
			pH		
			7.4–7.6	8.4–8.6	7.4–7.5 (BG-11)
LVMLG	179	1105	−5.41 ± 2.0	−2.48 ± 2.1	−0.06 ± 0.1
MVMLG	238	1469	−1.33 ± 0.3	−1.51 ± 1.7	−0.28 ± 0.4
HVMLG	495	3056	−0.89 ± 0.7	−10.14 ± 6.3	−0.91 ± 0.8

[a] M_w as informed by the manufacturer (Megazyme Ltd, Bray, Ireland). [b] DP is calculated from the equation $DP_w = M_w/M_0$, where M_0 = 0.162 kg mol^{-1}, molecular weight of MLGs monomer unit (glucose). [c] ζ-Potentials values should not be taken as absolute values but as estimates on the overall charge of the MLG solution since the measurement of ζ-potentials is not trivial due to the fast aggregation of MLG polymers. LVMLG, MVMLG, and HVMLG – barley low, medium, and high viscosity MLG, respectively.

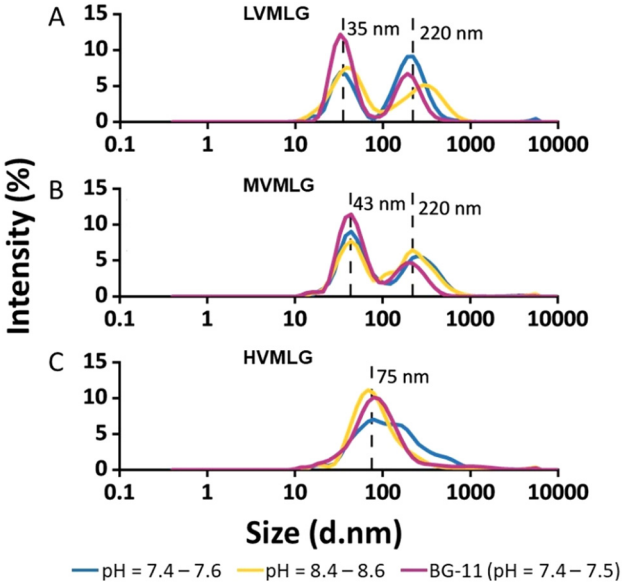

Fig. 2 Hydrodynamic diameters of MLGs. Size distributions of (A) LV-, (B) MV-, and (C) HVMLG determined by dynamic light scattering (DLS) measurements. The analyses were conducted for 0.01 wt% solutions in water at pH ranges of 7.4–7.6 (blue line) and 8.4–8.6 (yellow line), and in BG-11 growth medium (pink line) with neutral pH and approximately 20 mM ionic strength. Peak values in nm are indicated with dashed lines.

MLG molecular weight, and HVMLG displayed unimodal size distribution seen as a peak around 75 nm. Moreover, the number of individual chains in relation to agglomerated particles was higher in BG-11 regardless of MLG molecular weight, seen as a higher intensity of the smaller nm peaks.

As shown in Fig. 2, neutral MLG polymers have poor long-term stability. Indeed, polymer aggregates are detected even in freshly prepared MLG solutions, which supports the notion that the solubility of MLG polymers is limited indicating that polymer–polymer interactions are favoured over polymer–solvent interactions. The solubility of MLGs is therefore determined by a favourable free energy change when polymer segments are exchanged to solvent molecules during dissolution.[54] Given that MLG dissolution requires elevated temperatures *i.e.*, the process is endothermic, the solubility must be attributed to a gain in entropy during mixing of polymer and solvent.

MLGs, having relatively high molecular weights when considering hemicelluloses, behave as random coil polysaccharides in solution. Coupled with the asymmetric conformations, these features are likely to drive the aggregation and gel formation processes of MLGs.[11,43] It has been proposed that the interchain aggregates probably develop due to hydrogen bond formation between adjacent β-(1,4)-linked cellulose-like regions.[53,55,56] According to Stokes–Einstein diffusion theory, in diffusion-controlled transport where no shear flow is present, the rate of diffusion is lower the larger the polymer coil. As a result, coils formed by shorter MLG chains have higher mobility and they experience less spatial hindrance than the larger MLG coils, which increases possibilities for both translational (collision) and rotational diffusion (sticking).[53] Furthermore, the higher friction between polymer and solvent molecules retards the movement of larger molecules due to the entry of the viscosity effect as predicted in Smoluchowski coagulation model. In other words, the lower M_w MLG coils are more mobile and are more probable to associate with each other, which increases the chances for aggregate formation. The longer HVMLG chains remain as individual coils in solution as suggested in Fig. 2C. Similar observations were also made by Lazaridou *et al.*[43]

Additionally, the data suggests that increasing salt concentration has a positive effect on the solubility and stability of MLGs, which is seen as an increase in the amount of individual and non-aggregated MLG chains (Fig. 2). Based on ζ-potential measurements (Table 1), the overall charge of MLG system is even lower in higher salt concentration as compared with the systems in pure water at similar pH. The circumspect explanation could be that the long-range attractive interactions between the polymer chains are screened in the presence of high concentration of ionic species weakening the mobility of the MLG molecules in the electric field. Therefore, the polymer chains are not moving towards each other as efficiently, which increases MLG solution stability and less aggregates are formed. Another possible explanation is that the ionic species in the growth medium, such as nitrates, stabilise the electric double layer of MLGs, which otherwise is very weak. Furthermore, short-range repulsive hydration forces along with probable specific ionic interactions in the presence of nitrates may also contribute to the enhanced MLG dispersion stability.[57,58] Despite the efforts to understand solution properties of MLGs, the effect of salt on polymer solvency is not fully understood and further research is needed.

ζ-Potential and particle size measurements are by no means trivial. The poor long-term stability and low charge of MLGs hamper the polymer particle size and charge determinations. Despite preparing the solutions directly prior to running the samples and filtering them into the cuvettes, sometimes large standard deviations were detected. These findings express the importance on working with freshly prepared MLG solutions, as aggregation is strongly time-dependent phenomenon.

3.2. TCNF–MLG interactions and viscoelastic properties of adsorbed MLG layers – Polymers at interfaces

Adsorption of MLG on TCNF. To understand MLG binding on TCNF surfaces, and how MLGs contribute to TCNF gel wet strength, MLG adsorption on TCNF was studied using QCM-D. Fig. 3 shows changes in frequency and dissipation as a function of time (Fig. 3A and B), as well as their interrelations (Fig. 3C). Each different molecular weight MLG exhibited significant adsorption onto TCNF surfaces seen as clear negative change in frequency values (Fig. 3A). In pure water, final Δf values were approximately the same for all MLGs independent of molecular weight: −50 Hz for HVMLG and −45 Hz for both MV- and LVMLG. Overall, MLG molecular weight had only a minor effect on the adsorbed amount, whereas medium composition seemed to have a much bigger influence. The frequency change was only −20 Hz for LVMLG in BG-11 growth medium.

However, the different adsorbed MLG layers display different viscoelastic properties (Fig. 3B). Higher ΔD values were

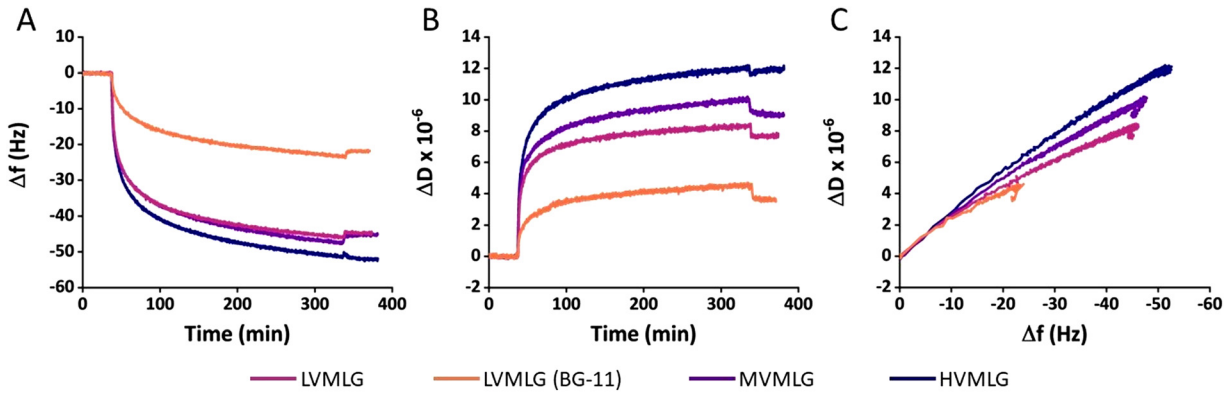

Fig. 3 Adsorption of MLGs on TCNF. Changes is (A) frequency, (B) dissipation factor, and (C) dissipation factor as a function of frequency during adsorption of 0.01 wt% MLG solutions on TCNF surfaces. A baseline for TCNF surfaces was first obtained, after which MLG solutions were introduced at around 30 min. Lastly, a rinsing step was applied at 350 min. Adsorption of LVMLG in both water and BG-11 growth medium is shown. 15 MHz, f_0 = 5 MHz, n = 3.

obtained with increasing MLG molecular weight as final levels of approximately 11, 9 and 7 $\times$ 10^{-6} were reached for HV-, MV-, and LVMLG, respectively. By simplified interrelation of the dissipation changes to viscoelastic properties of thin films, the results denote that layer softness increases in the order HVMLG > MVMLG > LVMLG as the amount of bound water increases. A more profound effect was again seen when the adsorption was conducted nutrient-rich growth medium. Change in dissipation of LVMLG in BG-11 attained 4 $\times$ 10^{-6}, which is only slightly above 50% of that in water. Moreover, plotting ΔD as a function of Δf allows concomitant comparison of how much energy the MLG layers bind during adsorption, *i.e.* how much energy the frequency changes correspond to. The slope of a $\Delta D/\Delta f$ curve is indicative of how dissipative a layer is and softening or packing of the layer is seen as a change in the slope. From Fig. 3C we can make an interpretation that MLG layers adsorbed from water are softer and more mobile than MLG layers adsorbed from BG-11, which are more densely packed. All in all, each MLG layer remained stable after rinsing *i.e.*, Δf and ΔD did not change significantly once pure solvent (either water or BG-11) was pumped through the cells after the adsorption on TCNF (Fig. 3A and B). These results are in line with the previously reported findings stating that adsorption of MLG on cellulose surfaces is irreversible.[11] We have established that MLGs behave as neutral polymers in aqueous environments. For TCNF with a similar carboxylate content to what was used here, a negative ζ-potential around -75 mV in water has been reported.[59] Regarding TCNF–MLG interactions, these findings indicate that the attribution of electrostatic interactions to adsorption of neutral MLG chains on the negatively charged TCNF surface is negligible *i.e.*, the driving force for adsorption must be non-electrostatic in nature. The unspecific binding suggests the mechanism of adsorption to be entropy-driven.[60] Therefore, binding is likely promoted by an increase in entropy that is gained by the loss of preferential polar interactions when water molecules at the TCNF–liquid interface are released into solution during MLG binding to the surface to minimise the change in Gibbs free energy.[60,61]

Interfacial rheology of the adsorbed MLG layers on TCNF. The viscoelastic properties of adsorbed MLG layers were interpreted using a model where the layer is presented as a single Voigt element.[41] The density and thickness of the layer are assumed uniform, and the layer is assumed to be deposited on a solid surface in contact with a purely viscous solvent. The Voigt-model was fitted to the 0.01 wt% MLG Δf and ΔD adsorption data. The fitting was done using data from several overtones. The results are shown in the ESI† (Fig. S2). Fig. 4 presents the evolution of shear viscosities (η_f), shear elastic moduli (μ_f), and hydrodynamic thicknesses (h_f) as a function of the adsorption time for the different MLG layers corresponding to the fittings. It is evident that all MLG layers adsorbed from pure water display similar rheological behaviour. The η_f (Fig. 4A) and μ_f (Fig. 4B) values reached levels of $\sim$1200 μPa s and 4 kPa, respectively, regardless of MLG polymer size. In nutrient rich growth medium, the adsorbed layer attains higher shear viscosity and shear elastic modulus values ($\sim$1300 μPa s and 12 kPa) pointing towards more densely packed and strongly bound LVMLG layer formed on TCNF surface. The final hydrodynamic thickness (h_f) values (Fig. 4C) for LV-. MV-, and HVMLG varied within 50–70 whereas the thickness of the LVMLG layer in BG-11 reduced to less than half of its thickness in pure water ($\sim$20 nm).

Viscoelastic modelling of the QCM-D data provides a tool for interpretation of adsorbed mass and structural changes in the adsorbed layers. In the context of this paper, it enables comparison of thin film rheology to rheological properties of the materials in bulk. As all ΔD values are $>1 \times 10^{-6}$ suggesting that TCNF–MLG layers are viscoelastic, it is reasonable to assume that the exploitation of Voigt model is warranted. Despite of its simplicity, the model fits the experimental adsorption data very well with the difference between measured data and calculated values being almost negligible for several overtones (Fig. S2, ESI†). It should be noted that even though the model is a useful estimate on the viscoelastic properties of the TCNF–MLG layers, the final calculated values are not to be taken as absolute values but as a tool enabling comparison of layer properties to each other.

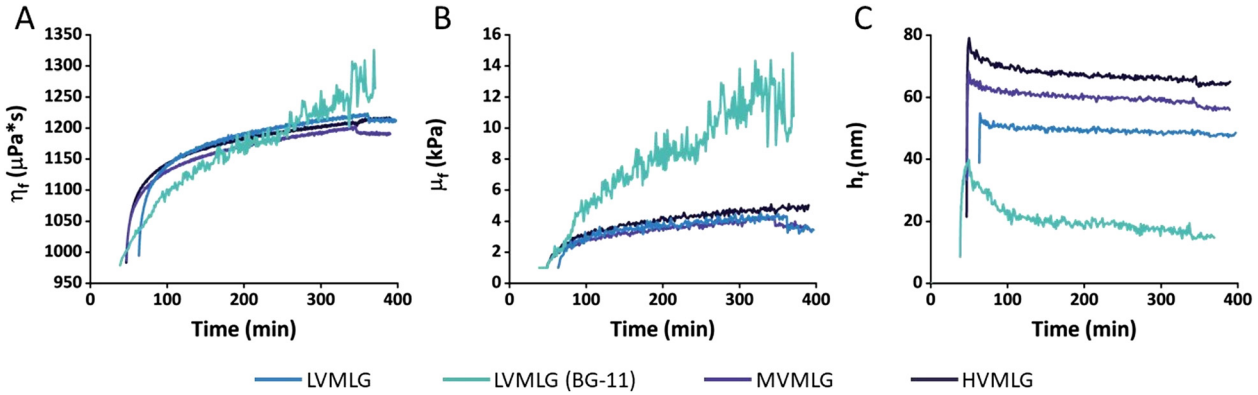

Fig. 4 Viscoelastic modelling of MLG adsorption data. (A) Shear viscosities (η_f), (B) shear elastic moduli (μ_f), and (C) hydrodynamic thicknesses (h_f) of the different MLG layers as a function of time obtained *via* fitting the the Voigt model to the adsorption data. Values for LVMLG in both water and BG-11 growth medium are shown. 15 MHz, f_0 = 5 MHz, n = 3. Assumed layer density 1.05 g cm^{-3}.

Dry areal mass determination of the MLG layers. The frequency responses of the different MLG layers were also recorded at the solid–air interface with the QCM-D device to analyse the dry areal mass changes before and after the MLG adsorption. The approach allows us to exclude the mass changes due to bound water detected during the adsorption process. The Δf and ΔD values recorded at solid–air interface are collected in the ESI† (Table S1). When dissipation changes between dry surfaces remain sufficiently low ($<1 \times 10^{-6}$) suggesting fully elastic layers, changes in areal mass can be calculated with the Sauerbrey equation (eqn (1)).

Fig. 5 shows changes in areal mass (Δm) of spincoated TCNF surfaces and subsequent MLG layers adsorbed on the TCNF surfaces. For LVMLG, two different layers are shown: one adsorbed in water and one in BG-11 growth medium. Areal mass changes due to MLG adsorption on TCNF reached approximately 400 ng cm^{-2} for both LVMLG and MVMLG, which is as expected due to their moderately similar M_w and DP values (Table 1). HVMLG being twice as large as MVMLG yields two times higher dry areal mass change of ~800 ng cm^{-2}. Interestingly, significantly higher dry mass of LVMLG was generated from nutrient rich medium being as high as 1200 ng cm^{-2}, which is approximately three times higher than the areal mass adsorbed from pure water. Furthermore, AFM imaging, which was used to probe the coverage, topography, and surface roughness of the dry TCNF–MLG layers, reveals

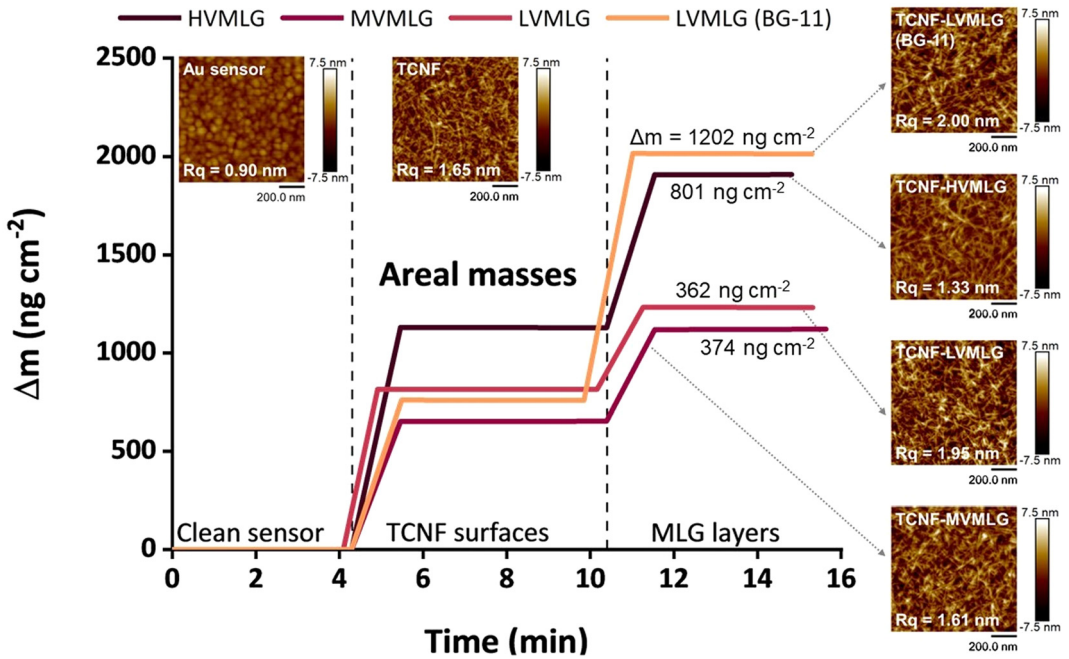

Fig. 5 Adsorbed MLG layers at the solid–air interface. Areal masses of clean sensors, added TCNF layers, as well as different MLG layers on TCNF surfaces. 15 MHz, f_0 = 5 MHz, n = 3. Layer density assumed as 1.05 g cm^{-3}. Final Δm between TCNF and TCNF–MLG surfaces are given. 1 × 1 μm AFM height images of the corresponding surfaces are included for visual representation and the clean Au sensor is shown as a reference. The images were flattened and analysed with NanoScope Analysis software (Bruker), and the root-mean-square roughness (R_q) values of each surface are embedded in the images.

that all different surfaces appeared to be even in coverage and the height images show only minor topological differences (AFM height images in Fig. 5). No MLG agglomerates were detected pointing towards the uniform thickness and density of the adsorbed layers that is a prerequisite for the viscoelastic treatment of the adsorbed layers by the Voigt model.

Structural representation of the TCNF–MLG systems. Fig. 6 schematically summarises the suggested conformational details of the MLG polymers in solution and once adsorbed on to the TCNF interface. The QCM-D data along with the viscoelastic modelling revealed that all MLGs form relatively thick hydrogels on nanocellulose surface, and the larger the polymer chains, the thicker the hydrogel. Based on the DLS measurements, both LV- and MVMLG dispersions contain both individual polymer chains and aggregated particles, while individual particles were dominating in the HVMLG dispersion (Fig. 2). The hydrodynamic diameters of the individual MLG polymer chains in aqueous solution (35, 43, and 75 nm for LV-, MV-, and HVMLG, respectively) roughly follow the same order and magnitude with the hydrodynamic thickness values (50, 60, and 70 nm as shown in Fig. 4C). This indicates that only the non-agglomerated MLG chains adsorb on the TCNF surfaces as depicted in Fig. 6A–C. This is well in accordance with the AFM images shown in Fig. 5 supporting the formation of uniform MLG layers. Only a minor liquid flow is present in the QCM-D chambers, and the adsorption process can be considered to be governed by the same principles as diffusion-controlled transport *i.e.*, the smaller particles migrate faster to the TCNF surfaces as previously discussed in the system describing the adsorption of cationic starch with a broad size distribution.[62] Larger aggregates hence seem to remain in solution as the individual chains quickly occupy the available binding sites.

Especially the longer HVMLGs contain segments forming internal loops and coils protruding out into the solution phase. In aqueous environments, water molecules are likely to strongly interact with the loops and coils keeping water molecules trapped inside the layer structure. Consequently, the amount of water in the MLG layer increases with the M_w of the MLG polymer, which is reflected as larger dissipation values and increased thickness corresponding to softer layers. The shorter LV- and MVMLGs, in contrast, form more stable and rigid layers with less incorporated water molecules.

The growth media had a highly pronounced effect on the LVMLG solution properties, adsorption properties, and, especially, the rheological properties of the thin films (Fig. 6D and E). The ions in BG-11 stabilised the LVMLG solutions, seen as an increase in the amount of individual polymer chains

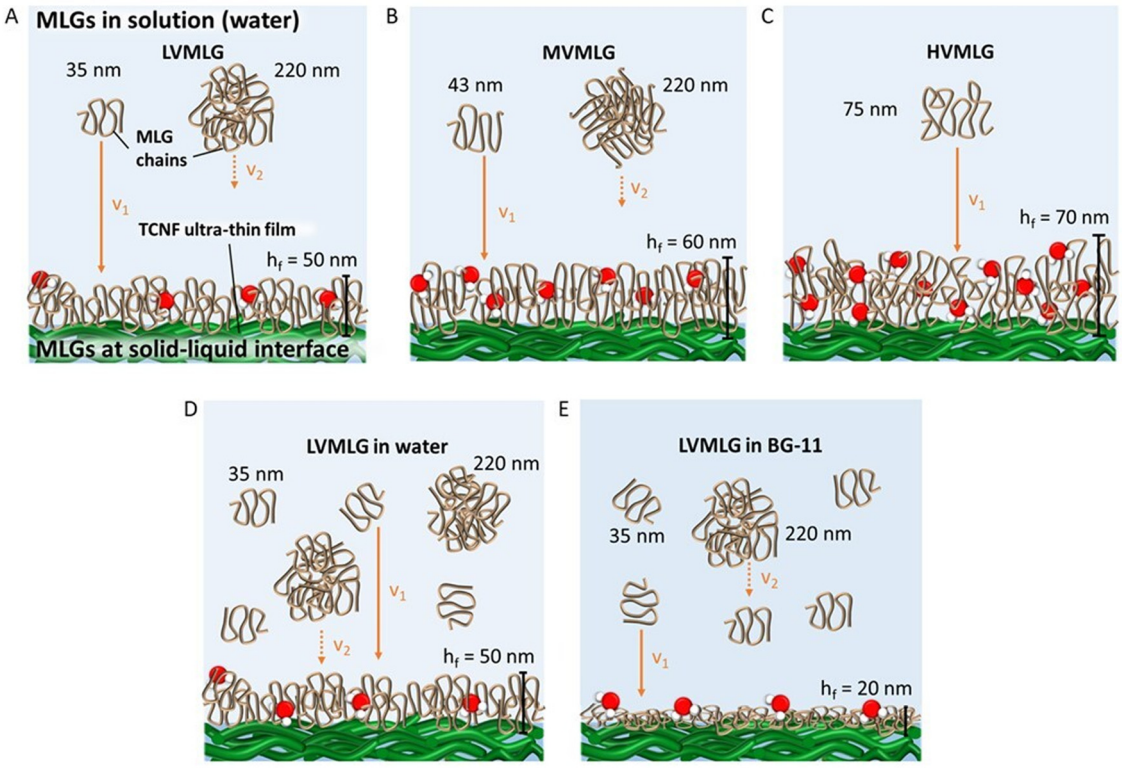

Fig. 6 Schematic representation of MLG polymers in solution and at the solid–liquid nanocellulose (TCNF) interface. (A) LV- and (B) MVMLG solutions contain both individual chains and agglomerated particles. In a diffusion-controlled system, the smaller particles migrate faster to the surface and the larger aggregates stay in solution. v_1 and v_2 along with the orange arrows represent the diffusion rates of individual and agglomerated MLG chains ($v_1 > v_2$). Red-and-white objects represent water molecules trapped inside the layers. For the sake of clarity, free water molecules are excluded. (C) Longer HVMLG chains with internal loops and coils form even thicker layers with more bound water. In comparison to LVMLG in water (D), in BG-11 (E) the polymer chains adsorb in a flatter conformation allowing a denser layer to be formed. Water molecules cannot penetrate into the structure, even though still associated with the layer. As a result, the obtained layers are much thinner.

compared to agglomerated polymers (Fig. 2). Demonstrated by the accumulation of a higher relative areal mass on the sensor surface (Fig. 5), adsorption of LVMLG in BG-11 is promoted. Arumughan *et al.*[63] recently showed that this is likely caused by the anion specific interactions resulting mainly from the nitrate ions present in the medium: chaotropic ions, such as nitrate,[58] accumulate near the chaotropic cellulose surface[64] altering the orientation of water molecules at the interface. The release of these unfavourably organised water molecules from the interface during adsorption generates a higher entropy gain that further promotes adsorption. MLGs also express self-affinity as shown by the aggregation behaviour present in aqueous solutions (Fig. 2), which combined with possible conformational changes could lead to formation of internal connections and exclusion of water molecules from the structure. In other words, the TCNF surface can accommodate more MLG molecules, allowing a higher dry mass to be built on top of the nanocellulose layer. Overall, the increased electrolyte concentration due to the presence of ionic species in the growth medium enables MLG chains to pack more densely in BG-11 (Fig. 6E) than in water (Fig. 6D), attributing to the formation of stronger, more stable, rigid, and flatter layers from BG-11.

In terms of the overall viscoelastic nature of the TCNF–MLG thin films, the μ_f values calculated using the Voigt model in kPa (10^3 × Pa) range are substantially higher in scale than the η_f values in μPa s (10^{-6} × Pa s), which indicates that the MLG layers all exhibit predominantly elastic character. As a reference, μ_f values in 10^5 Pa range have been obtained for cationic starches.[62] In comparison, the elastic moduli of MLG layers are lower. As the hydrodynamic thicknesses are overall rather high, all adsorbed MLG layers still show notable softness and viscoelastic character associated with strong water binding ability. The notable association of the adsorbed layers with water is in line with previous research reporting the significant role of water at hemicellulose–cellulose interfaces.[5]

To the authors' knowledge, there is little existing literature regarding MLG modelling that these results could be compared to. Kiemle *et al.*[11] reported estimated layer thicknesses of 15 nm when investigating adsorption of 0.01 wt% MVMLG solutions onto regenerated cellulose surfaces at approximately 20 mM ionic strength, however, in sodium acetate instead of BG-11. Our results showed a thickness of approximately 20 nm for LVMLG in the growth medium. The experimental condition used by Kiemle *et al.* (T = 48 °C, pH 5.5) differ from our conditions. In addition, the molecular weight of MLG in their studies was different, making direct comparison challenging. Nevertheless, the thickness obtained for LVMLG here seems realistic despite being a little higher than what was obtained for MVMLG at similar ionic strength.

3.3. Effect of MLG polymer size and concentration on matrix wet strength

Rheological measurements enable analysis of material behaviour under shear stress, which several papers list as a substantial challenge in photobioreactors.[65–67] To optimise the grade and amount of MLG in the TCNF-based hydrogel scaffold for mechanical stability and durability in submerged production conditions, small deformation oscillatory rheology was used. The aqueous conditions for wet strength determination were obtained by letting the samples swell overnight in water/BG-11 prior to the measurements. Fig. 7 displays critical stress values of self-standing MLG-Ca^{2+}-TCNF hydrogel films in Pa as a function of MLG concentration. Due to the nature of the samples and the measurement,[51] high variance in both was seen even though several replicates were measured, making it difficult to find considerable differences between the yield behaviour of the matrices with different molecular weight MLGs. Generally, however, it seemed that increasing the amount of MLG decreased the wet strength *i.e.*, 0.01–0.05 wt% MLG additions yielded better results than the higher concentrations. Also, it seemed that with LVMLG a higher amount was required to reach similar critical stresses that were reached already at 0.01 wt% with HV- and MVMLG. Overall, the wet strengths of all MLG-Ca^{2+}-TCNF hydrogel films were comparable to the previously reported TCNF-based matrix formulation with synthetic PVA.[22] Matrices with 0.1–0.2 wt% HVMLG were omitted from the rheological investigation due to lower biological compatibility based on preliminary visual assessment (Fig. S3, ESI†) and because the higher MLG concentrations were not expected to benefit the mechanical properties. The rest properties of the MLG-Ca^{2+}-TCNF matrices are additionally included in the ESI† (Fig. S4, ESI†).

As seen in the QCM-D experiments, the irreversible adsorption of MLGs onto TCNF proposedly leads to so-called polymer entanglement, meaning that MLGs physically bridge the cellulosic network.[11] These same interactions are assumed to be present also in bulk, meaning that the viscoelastic properties of the thin films are reflected to the bulk rheological properties of

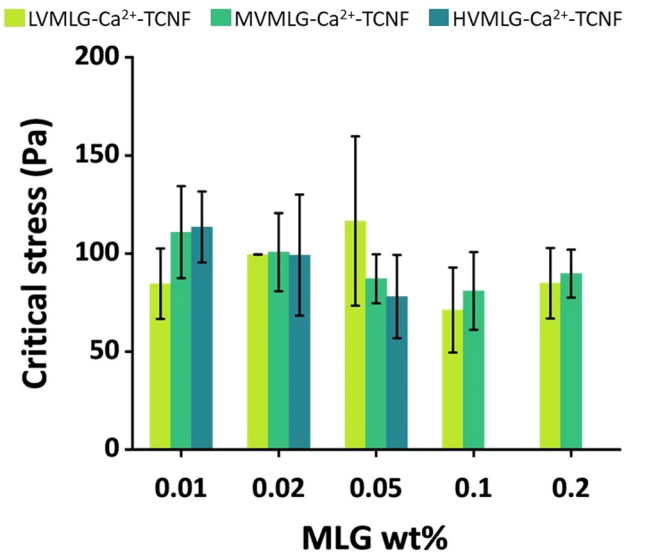

Fig. 7 Wet mechanical properties of self-standing MLG-Ca^{2+}-TCNF hydrogel films. Critical stress values of the matrices with LV-, MV-, and HVMLG in 0.01–0.2 wt% concentrations. Standard deviations from at least five replicate measurements are shown.

MLG-Ca^{2+}-TCNF matrices. However, a few important considerations need to be addressed.

First, the mechanical properties of the colloidal hydrogel matrix are attributed to properties of both TCNFs and the interlaced MLGs, which intrinsically have very different network structures.[12] Pure TCNFs are rather rigid structures in comparison to the more flexible MLG chains having an irregular shape due to the β-(1,3)-linkages in their backbone. When extended, the length of a (HV)MLG chain in comparison to a cellulose fiber can be a few times higher. Consequently, a network containing both TCNF and MLG is generally likely to be softer in nature than a TCNF network by itself, despite being more stable in an aqueous environment, and the softness increases the longer the interlaced MLG chains are and the more the system contains MLG.[12] Secondly, the ratio of TCNF to MLG is substantially higher in the hydrogels in comparison to the thin films investigated by the surface sensitive techniques. The matrix network mainly consists of the more rigid TCNFs with small amounts of interlaced MLGs. Therefore, the softening effect of MLGs is not as prominent as it could be if the amount of MLG in the matrix was increased significantly. Moreover, the MLG-Ca^{2+}-TCNF hydrogel films are dried during the preparation procedure. With areal masses, the total removal of water was seen to have a profound effect on the interactions in the TCNF–MLG network. Even though the hydrogel matrices are dried to a much lesser extent, the rheological properties may be affected by the process. Lastly, only molecular weight effects were investigated with the surface sensitive techniques. As shown by the rheology results, concentration is another factor influencing the viscoelastic properties and wet strength of the MLG-Ca^{2+}-TCNF matrices.

It is also important to note that all the hydrogel films studied in this paper also contained divalent Ca^{2+} cations, as di- and multivalent ions have been shown to have a strong effect on wet mechanical stability of TCNF-based networks.[30,51,68] In fact, the TCNF–MLG formulations discussed here did not form self-standing hydrogels without the Ca^{2+} ions (Fig. S5, ESI†). Differences in wet strength and yielding behaviour of the matrices, however, likely arise from the MLG component as all hydrogels were allowed to saturate with Ca^{2+} ions and it can be assumed that MLGs do not interact with Ca^{2+} ions due to their neutral charge.

The dissipation monitoring and modelling of TCNF–MLG thin films discussed in Section 3.2 indicated that larger MLG polymer sizes contribute to formation of softer layers than the shorter ones. Thus, one could expect HVMLG-Ca^{2+}-TCNF hydrogel films to have softer mechanical properties than the matrices with the other two MLGs. However, drying likely allows interactions with water to be replaced with particle–particle interactions. This effect is more pronounced with longer MLG chains containing internal loops and coils with multiple interaction sites that can attach onto several TCNF fibrils once bound water molecules are expelled from the structure. As a result, mechanical properties of the matrices with the higher molecular weight MLGs appear to be slightly better in comparison to LVMLG-Ca^{2+}-TCNF when the MLG concentration is low. When the concentration is increased, the presence of the irregular, interlaced MLG chains seems to result in softening of the network. Again, this effect is more pronounced the longer the MLGs are. Additionally, increasing the MLG concentration may cause entanglement and coiling of the long polymer chains with each other resulting in larger local MLG aggregates that soften the overall matrix network structure.

On the other hand, at a constant concentration, the number of individual polymer chains per mass unit is higher for MLGs with lower molecular weight. In other words, the number of chains interacting with TCNF fibrils likely increases even though there are fewer interaction sites per chain. In addition, surface interaction studies showed adsorption of LVMLG on TCNF to result in more rigid layers. At very low MLG concentrations, these features are probably less prominent and the longer polymer chains may yield better matrix wet mechanical properties. However, when the concentration is raised a little (to 0.02–0.05 wt%), LVMLG-Ca^{2+}-TCNF matrices display slightly better wet strength. This increase in concentration may bring a sufficient amount of LVMLGs in contact with TCNFs allowing a mechanically stable network to be established. Further increase of MLG concentration seems to have the same effect as with the higher molecular weight MLGs, *i.e.*, the TCNF-based network appears to lose some of its rigidity as the amount of the softer polymeric component in the matrix increases.

The effect of medium composition and incorporation of cells on matrix wet strength was also investigated, and the rheological properties MLG-Ca^{2+}-TCNF hydrogel films prepared in BG-11 with and without Synechocystis cells are included in the ESI† (Table S2 and Fig. S6). Unlike with the thin films, interpretation of the results at bulk level was more challenging and clear trends were difficult to observe due to heterogeneity of the samples and possible artefacts resulting from sensitivity of the measurement. As for the long-term stability of the hydrogel scaffolds with entrapped cells, while all MLG-Ca^{2+}-TCNF matrices remained stable in BG-11 for almost two weeks, LVMLG-Ca^{2+}-TCNF showcased superior performance in comparison to the other two matrices and retained its mechanical integrity for over 50 days in submerged conditions (Fig. S7, ESI†). Additionally, the strong interactions with TCNF observed for LVMLG in the nutrient rich growth medium as shown by the interfacial studies (Fig. 4–6) also support the choice of LVMLG to be used in the scaffold formulation. Hence, we chose to test the performance and productivity of LVMLG-Ca^{2+}-TCNF in ethylene production. The 0.05 wt% concentration was used as it showed slightly more promising results than the other concentrations.

3.4. Biological compatibility of scaffold and ethylene production by cyanobacteria entrapped in MLG-Ca^{2+}-TCNF matrices

The long-term biocompatibility of MLG-Ca^{2+}-TCNF matrices was assessed by entrapping wild-type Synechocystis cells in the hydrogel thin films and monitoring the cells' photosynthetic activity periodically during cultivation under normal room temperature and light conditions. The samples contained

HV-/MVMLG and LVMLG in 0.01 wt% and 0.05 wt% concentrations, respectively. Fig. 8A shows that the cells retained their photosynthetic activity in the LVMLG-Ca^{2+}-TCNF hydrogel for over 50 days. In fact, cells inside the MV- and HVMLG-Ca^{2+}-TCNF matrices also showcased good photosynthetic activities after almost two weeks. However, the monitoring was stopped as the samples started to deteriorate. It has been shown that the cells lose their photosynthetic activity if deprived of nutrients, such as N, S, P, and Ci amongst others, and that their photosynthetic apparatus is susceptible to light, requiring constant recovery.[69–74] Overall, these results indicate that nutrients are efficiently distributed inside the matrix and that the material supports long-term cell viability, *i.e.*, the hydrogels are biocompatible.

Moreover, the performance of the MLG-Ca^{2+}-TCNF scaffolds in bioproduction was evaluated using Synechocystis *efe* strain, which was specifically engineered for the photosynthetic production of ethylene.[45,46] The cells were entrapped in MLG-Ca^{2+}-TCNF films with LVMLG in 0.05 wt% concentration. The cells were entrapped at very low cell density and the fabricated films were allowed to adapt for 3 days in BG-11 medium under 1% CO_2 in an air atmosphere. As shown in Fig. 8B, MLG-Ca^{2+}-TCNF films demonstrated a dramatic increase in the cell density (determined by the change in Chl content) after 3 days of submerged cultivation. In addition to supporting photosynthetic activity, the increased cell density also supports the notion that the matrix is biocompatible with cyanobacteria. Interestingly, the Chl content of the films determined after 3 days of cultivation depended exponentially on the film thickness (Fig. 8C). As demonstrated in Fig. 8D, the immobilised cells were capable of producing ethylene for 5 days under submerged cultivation conditions. The overall ethylene production yield increased with the increase of the film thickness and was highest in 2 mm-thick films due to a high initial biomass content (Fig. 8C). At the same time, the specific ethylene production yield (calculated per mg Chl) showed almost similar dependence, but the differences were not statistically significant (Fig. 8E). Moreover, the specific activity showed a tendency to increase with increasing film thickness.

The Synechocystis *efe* strain synthesises ethylene thanks to the over-expressed ethylene-forming enzyme (Efe) from *Pseudomonas syringae*.[75] The process depends on photosynthetic CO_2 fixation and thus, requires inorganic carbon supplementation in the form of CO_2 or bicarbonate and moderate (10–100 μmol photons m^{-2} s^{-1}) illumination.[21] It has been shown that the entrapment of Synechocystis *efe* cells within thin Ca^{2+}–alginate films improves the ethylene production yield and the long-term catalytic performance of the entrapped cells for up to one month under semi-wet cultivation compared to suspension cultures.[21] However, Ca^{2+}–alginate films showed low mechanical stability under high (above 200 mM) bicarbonate loadings and thus, were unsuitable for submerged production.[22] On the

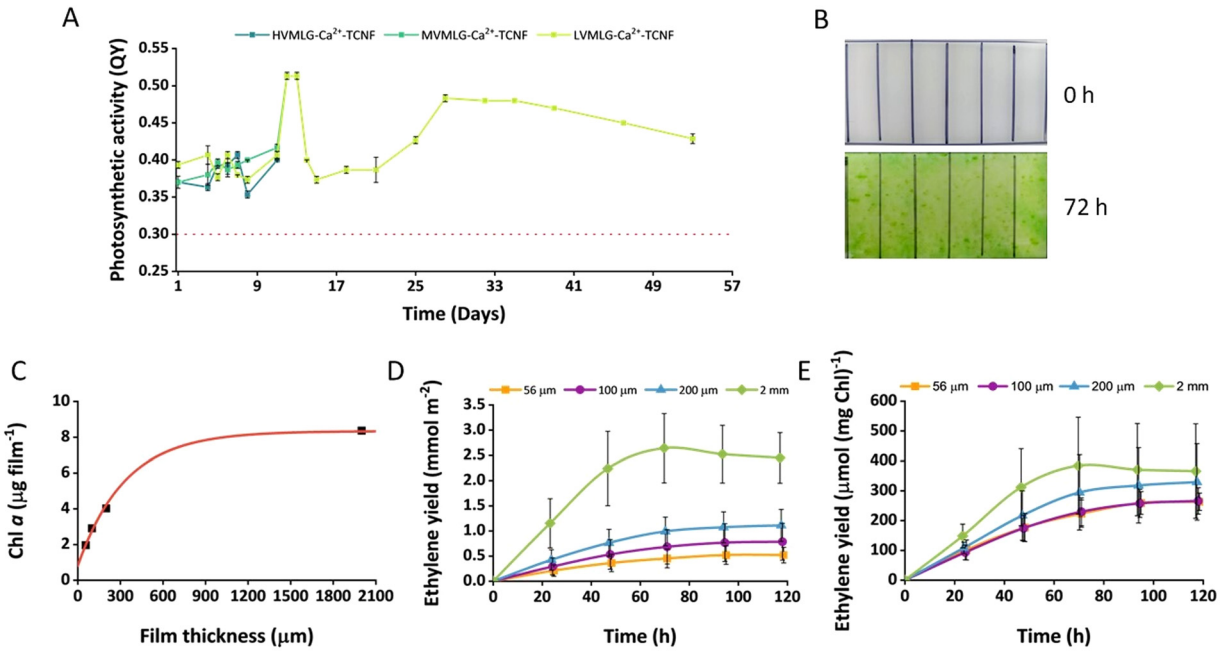

Fig. 8 Cell fitness of wild-type Synechocystis and biocatalytic performance of ethylene-producing Synechocystis *efe* cells entrapped within thin-layer MLG-Ca^{2+}-TCNF matrices under submerged cultivation. (A) The long-term viability of the wild-type cells in the nanocellulose-based scaffolds was monitored *via* photosynthetic activity. The given values are averages measured from three replicates and standard deviations are shown. The dashed red line shows the approximate value (0.3) below which the cells' fitness was considered as significantly affected. (B) For ethylene production experiments, the thin LVMLG-Ca^{2+}-TCNF films with Synechocystis *efe* (*efe* films) were adapted in BG-11 medium under 1% CO_2 in air atmosphere for 3 days. The change in the cell density of *efe* films after 3 d adaptation. 100 μm-thick film is shown as an example. (C) Dependence of Chl content of the *efe* film on the film thickness after 3 d adaptation. (D) Ethylene production yields by the *efe* films with different thicknesses. (E) Specific ethylene production yields by the *efe* films normalised to the total Chl content of the film. Values are the mean of 6 independent replicates and standard deviations are included.

other hand, entrapment of cyanobacterial cells in the self-standing PVA-Ca^{2+}-TCNF films resolved the problem.[22] We expected a similar result from MLG-Ca^{2+}-TCNF formulations.

The all-polysaccharidic MLG-Ca^{2+}-TCNF films were mechanically stable, and the cell density was sufficient for checking ethylene production after the three-day adaptation period. The exponential dependency between film Chl content and film thickness indicates that cell growth is limited by the distribution of nutrients (and/or CO_2) within the thicker films. We exclude a significant light limitation since the immobilised cultures can reach much higher cell densities under the same illumination conditions (but during a longer growth period). Additionally, the tendency of the specific activity to increase in the thicker films suggests that the process is not light-limited under these cultivation conditions, while the limitation of biomass formation results in slightly better ethylene productivity. In general, the ethylene production capacity of the cells during submerged cultivation conditions for 5 days is comparable to the data obtained previously.[22] The specific ethylene production activity by the MLG-Ca^{2+}-TCNF films was higher than in Ca^{2+}–alginate films under semi-wet cultivation,[21] as well as Ca^{2+}–alginate hydrogel and PVA-Ca^{2+}-TCNF films under submerged cultivation.[22] Thus, MLG-Ca^{2+}-TCNF matrices have the potential for engineering SSPCFs for photosynthetic production of chemicals and biofuels.

4. Conclusions

This work aimed to fabricate strong, biocompatible hydrogels from plant cell wall components. Obtaining all polysaccharide-based materials with sufficient mechanical performance in challenging aqueous and physiological conditions is not a trivial task though. In this research, we have shown that the interactions between the polysaccharidic components, nanocellulose and MLG, are strong enough to generate a scaffold for solid-state photosynthetic cell factories with sufficient wet strength in addition to being biocompatible and enhancing the viability of the cyanobacterial cells. Moreover, the ethylene production experiments showcase that the scaffold has the potential for bioproduction in submerged conditions. As a plant cell wall component and natural polymer, MLG offers a clear advantage in terms of biodegradability and end-of-life in comparison to fossil-based alternatives, such as PVA, as a structural component of the 3D SSPCF platform, allowing tailoring of the mechanical properties and water interactions of the matrix architecture.

Conflicts of interest

There are no conflicts to declare.

Acknowledgements

This project has received funding from the European Union's Horizon 2020 research and innovation programme under grant agreement No. 899576 and the Academy of Finland project #322752/#322754. S. A. was funded by the Academy of Finland grant #326262/311608. The authors acknowledge the support from the Academy of Finland funded flagship programme FinnCERES Materials Bioeconomy Ecosystem. This work made use of the Bioeconomy Facilities at Aalto University and VTT. Photosynthetic measurements and ethylene production experiments were performed in the University of Turku PhotoSYN infrastructure. We thank Teemu Suutari and Juan José Valle-Delgado for assistance with QCM-D and AFM measurements.

Notes and references

1 J. U. Fangel, P. Ulvskov, J. P. Knox, M. D. Mikkelsen, J. Harholt, Z. A. Popper and W. G. T. Willats, *Front. Plant Sci.*, 2012, **3**, DOI: 10.3389/fpls.2012.00152.
2 Y. Zhang, J. Yu, X. Wang, D. M. Durachko, S. Zhang and D. J. Cosgrove, *Science*, 2021, **372**, 706–711.
3 D. J. Cosgrove and M. C. Jarvis, *Front. Plant Sci.*, 2012, **3**, DOI: 10.3389/fpls.2012.00204.
4 J. P. Moore, M. Vicré-Gibouin, J. M. Farrant and A. Driouich, *Physiol. Plant.*, 2008, **134**, 237–245.
5 R. Cresswell, R. Dupree, S. P. Brown, C. S. Pereira, M. S. Skaf, M. Sorieul, P. Dupree and S. Hill, *Biomacromolecules*, 2021, **22**, 4669–4680.
6 A. Khodayari, W. Thielemans, U. Hirn, A. W. van Vuure and D. Seveno, *Carbohydr. Polym.*, 2021, **270**, 118364.
7 P. Eronen, M. Österberg, S. Heikkinen, M. Tenkanen and J. Laine, *Carbohydr. Polym.*, 2011, **86**, 1281–1290.
8 J. Lucenius, J. J. Valle-Delgado, K. Parikka and M. Österberg, *J. Colloid Interface Sci.*, 2019, **555**, 104–114.
9 T. M. Tenhunen, M. S. Peresin, P. A. Penttilä, J. Pere, R. Serimaa and T. Tammelin, *React. Funct. Polym.*, 2014, **85**, 157–166.
10 M. E. Vega-Sánchez, Y. Verhertbruggen, H. V. Scheller and P. C. Ronald, *Plant Signaling Behav.*, 2013, **8**, DOI: 10.4161/psb.23143.
11 S. N. Kiemle, X. Zhang, A. R. Esker, G. Toriz, P. Gatenholm and D. J. Cosgrove, *Biomacromolecules*, 2014, **15**, 1727–1736.
12 S. Arola, M. Ansari, A. Oksanen, E. Retulainen, S. G. Hatzikiriakos and H. Brumer, *Soft Matter*, 2018, **14**, 9393–9401.
13 J. C. Muñoz-García, K. R. Corbin, H. Hussain, V. Gabrielli, T. Koev, D. Iuga, A. N. Round, D. Mikkelsen, P. A. Gunning, F. J. Warren and Y. Z. Khimyak, *Biomacromolecules*, 2019, **20**, 4180–4190.
14 M. I. Khan, J. H. Shin and J. D. Kim, *Microb. Cell Fact.*, 2018, **17**, DOI: 10.1186/s12934-018-0879-x.
15 R. H. Wijffels, O. Kruse and K. J. Hellingwerf, *Curr. Opin. Biotechnol*, 2013, **24**, 405–413.
16 M. Jämsä, S. Kosourov, V. Rissanen, M. Hakalahti, J. Pere, J. A. Ketoja, T. Tammelin and Y. Allahverdiyeva, *J. Mater. Chem. A*, 2018, **6**, 5825–5835.
17 H. Leino, S. N. Kosourov, L. Saari, K. Sivonen, A. A. Tsygankov, E. M. Aro and Y. Allahverdiyeva, *Int. J. Hydrogen Energy*, 2012, **37**, 151–161.

18 G. Peers, *Trends Biotechnol.*, 2014, **32**, 551–555.
19 S. Kosourov, G. Murukesan, M. Seibert and Y. Allahverdiyeva, *Algal Res.*, 2017, **28**, 253–263.
20 S. N. Kosourov and M. Seibert, *Biotechnol. Bioeng.*, 2009, **102**, 50–58.
21 S. Vajravel, S. Sirin, S. Kosourov and Y. Allahverdiyeva, *Green Chem.*, 2020, **22**, 6404–6414.
22 V. Rissanen, S. Vajravel, S. Kosourov, S. Arola, E. Kontturi, Y. Allahverdiyeva and T. Tammelin, *Green Chem.*, 2021, **23**, 3715–3724.
23 H. Lee, D. Shin, J. Choi, C. S. Ki and J. Hyun, *Carbohydr. Polym.*, 2022, **290**, 758–767.
24 E. Kontturi, P. Laaksonen, M. B. Linder, Nonappa, A. H. Gröschel, O. J. Rojas and O. Ikkala, *Adv. Mater.*, 2018, **30**, 1703779.
25 M. C. Li, Q. Wu, R. J. Moon, M. A. Hubbe and M. J. Bortner, *Adv. Mater.*, 2021, **33**, 2006052.
26 K. Heise, E. Kontturi, Y. Allahverdiyeva, T. Tammelin, M. B. Linder, Nonappa and O. Ikkala, *Adv. Mater.*, 2021, **33**, 2004349.
27 M. C. Jarvis, *Philos Trans. R. Soc., A*, 2018, **376**, DOI: **10.1098/rsta.2017.0045**.
28 T. Saito, Y. Nishiyama, J. L. Putaux, M. Vignon and A. Isogai, *Biomacromolecules*, 2006, **7**, 1687–1691.
29 A. Walther, F. Lossada, T. Benselfelt, K. Kriechbaum, L. Berglund, O. Ikkala, T. Saito, L. Wågberg and L. Bergström, *Biomacromolecules*, 2020, **21**, 2536–2540.
30 H. Dong, J. F. Snyder, K. S. Williams and J. W. Andzelm, *Biomacromolecules*, 2013, **14**, 3338–3345.
31 M. Hakalahti, A. Salminen, J. Seppälä, T. Tammelin and T. Hänninen, *Carbohydr. Polym.*, 2015, **126**, 78–82.
32 M. Hakalahti, A. Mautner, L. S. Johansson, T. Hänninen, H. Setälä, E. Kontturi, A. Bismarck and T. Tammelin, *ACS Appl. Mater. Interfaces*, 2016, **8**, 2923–2927.
33 E. Chiellini, A. Corti, S. D'Antone and R. Solaro, *Prog. Polym. Sci.*, 2003, **28**, 963–1014.
34 H. V. Scheller and P. Ulvskov, *Annu. Rev. Plant Biol.*, 2010, **61**, 263–289.
35 W. Cui, P. J. Wood, B. Blackwell and J. Nikiforuk, *Carbohydr. Polym.*, 2000, **41**, 249–258.
36 J. R. Woodward, G. B. Fincher and B. A. Stone, *Carbohydr. Polym.*, 1983, **3**, 207–225.
37 R. A. Burton and G. B. Fincher, *Mol. Plant*, 2009, **2**, 873–882.
38 N. Böhm and W.-M. Kulicke, *Carbohydr. Res.*, 1999, **315**, 302–311.
39 S.-J. Kim and F. Brandizzi, *Plant Cell Physiol.*, 2021, **62**, 1839–1846.
40 P. J. Harris and G. B. Fincher, in *Chemistry, Biochemistry, and Biology of 1-3 Beta Glucans and Related Polysaccharides*, ed. A. Bacic, G. B. Fincher and B. A. Stone, Elsevier, 2009, ch. 4.6, pp. 621–654.
41 M. V. Voinova, M. Rodahl, M. Jonson and B. Kasemo, *Phys. Scr.*, 1999, **59**, 391–396.
42 Scandinavian Pulp, Paper and Board Testing Committee, SCAN-CM 65:02 Total acidic group content conductometric titration method, Stockholm, Sweden, 2002.
43 A. Lazaridou, C. G. Biliaderis and M. S. Izydorczyk, *Food Hydrocolloids*, 2003, **17**, 693–712.
44 R. Rippka, J. Deruelles, J. B. Waterbury, M. Herdman and R. Y. Stanier, *J. Gen. Microbiol.*, 1979, **111**, 1–61.
45 K. Thiel, E. Mulaku, H. Dandapani, C. Nagy, E. M. Aro and P. Kallio, *Microb. Cell Fact.*, 2018, **17**, DOI: **10.1186/s12934-018-0882-2**.
46 V. Carbonell, E. Vuorio, E. M. Aro and P. Kallio, *World J. Microbiol. Biotechnol.*, 2019, **35**, DOI: **10.1007/s11274-019-2652-7**.
47 M. Hakalahti, M. Faustini, C. Boissière, E. Kontturi and T. Tammelin, *Biomacromolecules*, 2017, **18**, 2951–2958.
48 P. Eronen, M. Österberg, S. Heikkinen, M. Tenkanen and J. Laine, *Carbohydr. Polym.*, 2011, **86**, 1281–1290.
49 M. S. Peresin, K. Kammiovirta, H. Setälä and T. Tammelin, *J. Polym. Environ.*, 2012, **20**, 895–904.
50 G. S. Tóth, V. Siitonen, L. Nikkanen, L. Sovic, P. Kallio, R. Kourist, S. Kosourov and Y. Allahverdiyeva, *Biotechnol. Biofuels Bioprod.*, 2022, **15**, DOI: **10.1186/s13068-022-02248-1**.
51 T. Levä, V. Rissanen, L. Nikkanen, V. Siitonen, M. Heilala, J. Phiri, T. C. Maloney, S. Kosourov, Y. Allahverdiyeva, M. Mäkelä and T. Tammelin, *Biomacromolecules*, 2023, DOI: **10.1021/acs.biomac.3c00261**.
52 H. K. Lichtenthaler, *Methods Enzymol.*, 1987, **148**, 350–382.
53 W. Li, S. W. Cui, Q. Wang and R. Y. Yada, *Food Hydrocolloids*, 2011, **25**, 189–195.
54 G. Fleer, M. A. Cohen Stuart, J. M. H. M. Scheutjens, T. Cosgrove and B. Vincent, *Polymers at Interfaces*, Chapman & Hall, London, 1993.
55 J.-L. Doublier and P. J. Wood, *Cereal Chem.*, 1995, **72**, 335–340.
56 J. R. Woodward, D. R. Phillips and G. B. Fincher, *Carbohydr. Polym.*, 1988, **8**, 85–97.
57 J. N. Israelachvili, *Intermolecular and Surface Forces*, Elsevier, 3rd edn, 2011, ch. 15, pp. 341–380.
58 K. P. Gregory, G. R. Elliott, H. Robertson, A. Kumar, E. J. Wanless, G. B. Webber, V. S. J. Craig, G. G. Andersson and A. J. Page, *Phys. Chem. Chem. Phys.*, 2022, **24**, 12682–12718.
59 Y. Okita, T. Saito and A. Isogai, *Biomacromolecules*, 2010, **11**, 1696–1700.
60 S. Lombardo and W. Thielemans, *Cellulose*, 2019, **26**, 249–279.
61 T. Benselfelt, E. D. Cranston, S. Ondaral, E. Johansson, H. Brumer, M. W. Rutland and L. Wågberg, *Biomacromolecules*, 2016, **17**, 2801–2811.
62 T. Tammelin, J. Merta, L. S. Johansson and P. Stenius, *Langmuir*, 2004, **20**, 10900–10909.
63 V. Arumughan, H. D. Özeren, M. Hedenqvist, M. Skepö, T. Nypelö, M. Hasani and A. Larsson, *ChemRxiv*, 2023, preprint, DOI: **10.26434/chemrxiv-2023-c02j8**.
64 N. Mittal, T. Benselfelt, F. Ansari, K. Gordeyeva, S. V. Roth, L. Wågberg and L. D. Söderberg, *Angew. Chem.*, 2019, **131**, 18735–18742.
65 M. J. Barbosa, Hadiyanto and R. H. Wijffels, *Biotechnol. Bioeng.*, 2004, **85**, 78–85.
66 C. Gudin and D. Chaumont, *Bioresour. Technol.*, 1991, **38**, 145–151.

67 C. Posten, *Eng. Life Sci.*, 2009, **9**, 165–177.
68 T. Benselfelt, M. Nordenström, M. M. Hamedi and L. Wågberg, *Nanoscale*, 2019, **11**, 3514–3520.
69 V. Kumaresan, F. Nizam, G. Ravichandran, K. Viswanathan, R. Palanisamy, P. Bhatt, M. V. Arasu, N. A. Al-Dhabi, K. Mala and J. Arockiaraj, *Algal Res.*, 2017, **23**, 96–103.
70 S. Kosourov, H. Leino, G. Murukesan, F. Lynch, K. Sivonen, A. A. Tsygankov, E. M. Aro and Y. Allahverdiyeva, *Appl. Environ. Microbiol.*, 2014, **80**, 5807–5817.
71 R. Schwarz and K. Forchhammer, *Microbiology*, 2005, **151**, 2503–2514.
72 D. Kirilovsky, *Photosynth. Res.*, 2015, **126**, 3–17.
73 A. Latifi, M. Ruiz and C. C. Zhang, *FEMS Microbiol. Rev.*, 2009, **33**, 258–278.
74 A. Derks, K. Schaven and D. Bruce, *Biochim. Biophys. Acta, Bioenerg.*, 2015, **1847**, 468–485.
75 K. Nagahama, T. Ogawa, T. Fujii, M. Tazaki, S. Tanase, Y. Morino and H. Fukuda, *J. Gen. Microbiol.*, 1991, **137**, 2281–2286.